ELSEVIER

A numerical study of three-dimensional laminar natural convection in a vented enclosure

E. Yu and Y. Joshi
CALCE Electronic Packaging Research Center, and Department of Mechanical Engineering, University of Maryland, College Park, Maryland, USA

A three-dimensional numerical investigation of steady laminar natural convection in vented enclosures is carried out. A discrete flush-type heat source mounted on the substrate is used to simulate an electronic component. Four different vent locations are investigated. Combined natural convection in the air and conduction in the heat source, the substrate, and the enclosure walls are solved. Solutions are obtained for Rayleigh numbers ranging from 10^4 to 10^6, different substrate thermal conductivity ratios, and varied vent sizes. The calculation domain is extended beyond the cubic enclosure in *x*-, *y*-, and *z*-directions. Appropriate boundary conditions are prescribed on the extended computational domain. The resulting flow and temperature patterns are discussed. Also, the local and overall heat transfer from the heat source and the substrate, in terms of Nusselt numbers and the surface temperatures, are presented to illustrate the vent effects.
©1997 by Elsevier Science Inc.

Keywords: natural convection; partially open enclosures; vented enclosures; conjugate heat transfer

Introduction

Natural-convection air cooling of electronic components in vented enclosures is employed in many electronic systems. Proper placement of vents on enclosure walls can substantially enhance the cooling of components. The study of natural convection in vented enclosures is also very important in understanding the flow and temperature fields in many other engineering applications, such as solar collectors and fire spreading in rooms and corridors. A number of numerical studies have been reported on this problem, but these investigations are restricted to two-dimensional (2-D) configurations. To study the effects of vents in realistic applications, a three-dimensional (3-D) geometry must be considered.

Miyamoto et al. (1989) reported on a numerical study of laminar natural convection from a fully or partially open square cavity. Effects of inclination of the opening and cavity were studied. Chan and Tien (1985, 1986) investigated the laminar natural convection in a 2-D enclosure numerically and experimentally. An approximation of boundary conditions at the opening was presented. Angirasa et al. (1992) obtained the results for transient analysis of flow and thermal fields in the same geometry as that used by Chan and Tien, and the calculation was carried out based on an approximate boundary condition at the opening. Gebhart et al. (1988) discuss two approaches to handle the boundary conditions for calculating transport in partial enclosures. The first approach is to specify approximate boundary conditions at the openings, and the second one is to deal with the extended domain.

Abib and Jaluria (1988) investigated the effects of opening sizes and Rayleigh numbers in a 2-D configuration. It was found that the effect of the opening is not pronounced for low-Rayleigh numbers, but is significant for high Rayleigh numbers. They (Abib and Jaluria 1992, 1993) also studied the penetrative laminar convection and the generation of stable thermal stratification by turbulent flows in a partially open enclosure with a horizontally oriented heat source. Xia and Zhou (1992) presented the effects of dividers in a partially open cavity with Rayleigh number ranging from 10^4 to 10^6. It was found that the divider significantly decreases the heat transfer rate. Dehghan (1994) and Dehghan and Behnia (1996) made a detailed investigation of 2-D natural convection in discretely heated open top cavities. Natural convection in partitioned enclosures has been studied by Karki et al. (1992), Olson et al. (1990) and Kelkar and Patankar (1990). Some experimental results were also reported concerning this topic by Myrum (1990) and Sefcik et al. (1991) for 2-D vented enclosures.

In the present study, a 3-D numerical investigation of steady laminar natural convection air cooling of a single flush-type component in a vented cubic enclosure is reported. The calculation domain is extended beyond the enclosure configuration for clearly understanding the 3-D interaction between the heat source and the vents. The effects of locations of vents and vent sizes are investigated, as well as the thermal conductivity of the substrate. The solutions are obtained for a range of Rayleigh numbers. The local and overall heat transfer from the heat source and the

Address reprint requests to Dr. Y. Joshi, University of Maryland at College Park, CALCE Electronic Packaging Research Center and Department of Mechanical Engineering, College Park, MD 20742, USA.

Received 8 July 1996; accepted 13 February 1997

Int. J. Heat and Fluid Flow 18: 600–612, 1997
© 1997 by Elsevier Science Inc.
655 Avenue of the Americas, New York, NY 10010

0142-727X/97/$17.00
PII S0142-727X(97)00002-7

substrate, in terms of Nusselt numbers and the surface temperatures, are presented to illustrate the vent effects. Also, the flow and thermal patterns within the enclosure are presented.

Problem formulation

Geometry

The configuration under study is shown in Figure 1a. A flush heated region is located at the center of the substrate to simulate an electronic component. A uniform volumetric generation rate is assumed within the component. The substrate serves as a wall of the cubic enclosure of side L. All enclosure walls have a finite thickness to simulate the heat conduction within the enclosure case material. Five vent configurations have been considered. Three of these include a single vent, and the remaining two include two vents. The vent is treated as an opening without grills. The calculation domain is extended beyond the enclosure, as shown in Figure 1b. Because of the symmetry of the geometry with respect to the plane at $z = 0$, only half of the enclosure is employed for the present numerical calculations. The validity of this assumption was verified by running a full domain simulation for $\mathrm{Ra} = 10^6$. The computed flow and temperature fields were found to be entirely symmetric.

Governing equations

Combined natural convection in the air and conduction in the heat source, the substrate, and the enclosure walls are studied. The thermophysical properties and enclosure and heat source dimensions are kept fixed in the numerical computations. The Boussinesq approximation is invoked for the flow. Surface radiation may affect the flow and temperature fields, especially for large temperature differences between the heated and unheated walls. An estimation of radiation effects was performed, based on radiosity/irradiation approach by solving the combined natural convection and radiation. A summary of results is presented in Table 1. It is clear that for wall emissivities below 0.1 and for the temperature conditions applied, the radiation correction of temperature is less than 2.4%, and it can be decoupled from the conduction/convection analysis. A coupled radiation calculation is warranted for large wall emissivities and/or higher temperatures. In the present study, effects of venting on conduction and natural convection heat transfer are the focus, and the coupling

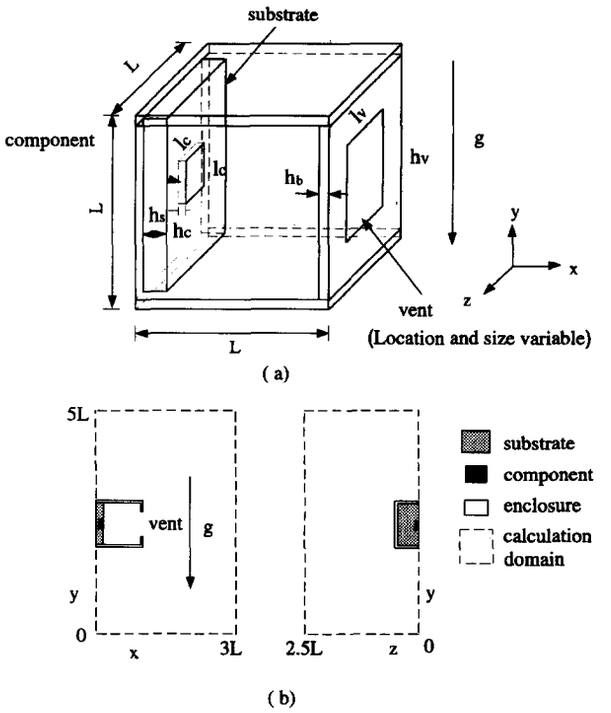

Figure 1 Geometry and calculation domain (a) geometry of the enclosure; (b) extended calculation domain

Notation

g	gravitational acceleration
h_c	thickness of component
h_s	thickness of substrate
h_b	thickness of enclosure wall
h_v	height of vent
k	thermal conductivity
l_c	length of component
l_v	width of vent
L	length of enclosure
M_{out}	nondimensional mass outflow rate
Nu	local Nusselt number
$\overline{Nu}$	average Nusselt number
p	pressure
Pr	Prandtl number
Q	heat generation rate
Ra	Rayleigh number
R_b	ratio of case thermal conductivity to fluid thermal conductivity
R_c	ratio of component thermal conductivity to fluid thermal conductivity
R_s	ratio of substrate thermal conductivity to fluid thermal conductivity
S_v	vent ratio $= h_v/(L - 2h_b)$
T	temperature
t, v, w	velocities in x-, y-, z-directions, respectively
x, y, z	Cartesian coordinate

Greek

α	thermal diffusivity of fluid
β	coefficient of thermal expansion
ε	emissivity
θ	nondimensional temperature
ν	kinematic viscosity
ρ	density of fluid

Subscripts

b	enclosure
c	component
f	fluid
s	substrate
v	vent

Table 1 Radiation effect for various surface emissivities of substrates at $Ra = 8.1 \times 10^5$, $S_v = 0.8$ (right side vented); $R_s = 7.7$; the surface emissivities are 0.6 for surrounding walls and 1.0 for the opening

Emissivity	0	0.05	0.1	0.5	1.0
Percentage of maximum temperature decrease	0%	1.1%	2.4%	10.7%	17.5%

of conduction, natural convection, and radiation is, therefore, not implemented. The dimensionless governing equations are:

Continuity:

$$\frac{\partial U}{\partial X} + \frac{\partial V}{\partial Y} + \frac{\partial W}{\partial Z} = 0 \tag{1}$$

x-momentum:

$$\frac{\partial (UU)}{\partial X} + \frac{\partial (VU)}{\partial Y} + \frac{\partial (WU)}{\partial Z} = -\frac{\partial P}{\partial X} + (\mathrm{Pr}/\mathrm{Ra})^{1/2}\left(\frac{\partial^2 U}{\partial X^2} + \frac{\partial^2 U}{\partial Y^2} + \frac{\partial^2 U}{\partial Z^2}\right) \tag{2}$$

y-momentum:

$$\frac{\partial (UV)}{\partial X} + \frac{\partial (VV)}{\partial Y} + \frac{\partial (WV)}{\partial Z} = -\frac{\partial P}{\partial Y} + (\mathrm{Pr}/\mathrm{Ra})^{1/2}\left(\frac{\partial^2 V}{\partial X^2} + \frac{\partial^2 V}{\partial Y^2} + \frac{\partial^2 V}{\partial Z^2}\right) + \theta \tag{3}$$

z-momentum:

$$\frac{\partial (UW)}{\partial X} + \frac{\partial (VW)}{\partial Y} + \frac{\partial (WW)}{\partial Z} = -\frac{\partial P}{\partial Z} + (\mathrm{Pr}/\mathrm{Ra})^{1/2}\left(\frac{\partial^2 W}{\partial X^2} + \frac{\partial^2 W}{\partial Y^2} + \frac{\partial^2 W}{\partial Z^2}\right) \tag{4}$$

Energy for air:

$$\frac{\partial (U\theta)}{\partial X} + \frac{\partial (V\theta)}{\partial Y} + \frac{\partial (W\theta)}{\partial Z} = (1/\mathrm{PrRa})^{1/2}\left(\frac{\partial^2 \theta}{\partial X^2} + \frac{\partial^2 \theta}{\partial Y^2} + \frac{\partial^2 \theta}{\partial Z^2}\right) \tag{5}$$

Energy for component:

$$\left(\frac{\partial^2 \theta}{\partial X^2} + \frac{\partial^2 \theta}{\partial Y^2} + \frac{\partial^2 \theta}{\partial Z^2}\right) + 1/(R_c H_c) = 0 \tag{6}$$

Energy for substrate and enclosure walls:

$$\frac{\partial^2 \theta}{\partial X^2} + \frac{\partial^2 \theta}{\partial Y^2} + \frac{\partial^2 \theta}{\partial Z^2} = 0 \tag{7}$$

The nondimensional parameters are defined based on the characteristic length l_c, the characteristic velocity $U_0 = (g\beta Q/k_f)^{1/2}$ and the heat generation rate Q, and they are as follows:

$$X = x/l_c \qquad Y = y/l_c \qquad Z = z/l_c \tag{8a}$$

$$H_c = h_c/l_c \; H_s = h_s/l_c \; H_b = h_b/l_c \; H_v = h_v/l_c \; L_v = l_v/l_c$$

$$L_X = L_Y = L_Z = L/l_c \tag{8b}$$

$$U = u/U_0 \qquad V = v/U_0 \qquad W = w/U_0 \tag{8c}$$

$$P = p/(\rho U_0^2) \qquad \theta = (T - T_a)/(Q/l_c k_f) \tag{8d}$$

$$\mathrm{Ra} = g\beta Q l_c^2/(\alpha v k_f) \qquad \mathrm{Pr} = v/\alpha \tag{8e}$$

The boundary conditions are applied to the enlarged calculation domain. The boundary at $X = 0$ is insulated. At $Z = 0$, a symmetry condition is employed. The four remaining boundaries are simulated to be free boundaries by specifying temperature and velocity instead of pressure. The approximation of the free-boundary conditions is similar to that suggested by Chan and Tien (1985) for 2-D flows. The final boundary conditions are as follows:

$$\frac{\partial \theta}{\partial X} = 0, U = 0, V = 0, W = 0, \quad \text{at } X = 0$$

$$\frac{\partial U}{\partial X} = 0, \frac{\partial V}{\partial X} = 0, \frac{\partial W}{\partial X} = 0, \quad \text{and}$$

$$\frac{\partial \theta}{\partial X} = 0 \quad \text{when} \quad U > 0, \theta = 0 \quad \text{when} \quad U \le 0, \quad \text{at}$$

$$X = 3L_X$$

$$\theta = 0, \frac{\partial U}{\partial Y} = 0, V = 0, \frac{\partial W}{\partial Y} = 0, \quad \text{at} \quad Y = 0$$

$$\frac{\partial U}{\partial Y} = 0, \frac{\partial V}{\partial Y} = 0, \frac{\partial W}{\partial Y} = 0, \quad \text{and}$$

$$\frac{\partial \theta}{\partial Y} = 0 \quad \text{when} \quad V > 0, \theta = 0 \quad \text{when} \quad V \le 0, \quad \text{at}$$

$$Y = 5L_Y$$

$$\frac{\partial \theta}{\partial Z} = 0, \frac{\partial U}{\partial Z} = 0, \frac{\partial V}{\partial Z} = 0, W = 0, \quad \text{at} \quad Z = 0$$

$$\frac{\partial U}{\partial Z} = 0, \frac{\partial V}{\partial Z} = 0, \frac{\partial W}{\partial Z} = 0, \quad \text{and}$$

$$\frac{\partial \theta}{\partial Z} = 0 \quad \text{when} \quad W > 0, \theta = 0 \quad \text{when} \quad W \le 0, \quad \text{at}$$

$$Z = 2.5L_Z$$

Table 2 Grid testing for the domain outside the enclosure; $Ra = 10^7$; Grid within the enclosure: $23 \times 22 \times 15$

	$33 \times 38 \times 23$	$38 \times 42 \times 25$	$42 \times 46 \times 28$
$\overline{Nu}$	19.493	19.915	19.976
Maximum component temperature	0.0158	0.0156	0.0155
Maximum wall temperature	0.00580	0.00585	0.00588
Maximum heat flux on the inner surface of the substrate	6.19×10^{-4}	6.45×10^{-4}	6.42×10^{-4}

The solutions were obtained for $L_x = 5$, $L_y = 5$, $L_z = 5$, $H_c = 0.3$, $H_s = 0.6$, $H_b = 0.1$. The width of the vent is fixed at $L_v = 2.5$, while the vent ratio S_v ranges from 0 to 1. The normalized thermal conductivities of the component and the enclosure walls are kept fixed at $R_c = 7692.3$ and $R_b = 38.5$, respectively. Two values of the thermal conductivity ratio of the substrate to fluid are employed: $R_s = 23.1$, corresponding to epoxy fiberglass, and $R_s = 5769.2$, corresponding to aluminum. These values apply to air as the working fluid.

Numerical approach

Numerical method

The governing equations for the conjugate problem are solved using SIMPLER algorithm detailed by Patankar (1980). The abrupt changes of thermal conductivities at the interface of two materials are handled by the harmonic mean formulation. The numerical solution is considered to be converged when the ratio of the maximum temperature change to the maximum temperature at that iteration is within 1×10^{-5}, the ratio of the maximum velocity change to the maximum velocity at that iteration is within 1×10^{-4}, and the residual of the energy equation for the whole domain is within 1%. The code is validated by solving for 3-D natural convection in a cubic enclosure with one hot wall, one cold wall, and four insulated walls. The results for Nu and maximum velocity were found to be within 1% and 2%, respectively, of those reported by Mallinson and de Vahl Davis (1977).

Grid testing

The adequacy of grids within and outside the enclosure was tested for $Ra = 10^7$, and the results are shown in Table 2 and Table 3. In testing of grids in the domain outside the enclosure, it was found that the fineness of grids in the domain below the bottom wall of the enclosure influenced the calculation results very slightly, so coarse grids are used there. In the domain above the top enclosure wall at $Y = 3L_Y$ and the domain to the right side of the enclosure wall at $X = L_X$, relatively finer grids are employed. A fine grid was also used near the solid surfaces. Near the inner surface of the substrate, a much finer grid was employed to capture the flow and thermal characteristics in the boundary layer. Overall, most of the compuatations were performed using a nonuniform grid of $33 \times 38 \times 23$, resulting in a $23 \times 22 \times 15$ grid pattern within the enclosure. Only for the small vent size case, more grids are used in the y-direction to study the vent effect.

Flow and temperature fields

Computations were carried out for the various cases identified in Table 4. In the following, flow and temperature results are displayed only within the enclosure for these cases.

Table 3 Grid testing for the domain within the enclosure, $Ra = 10^7$; grid outside the enclosure: $10 \times 16 \times 8$

	$33 \times 38 \times 23$	$37 \times 46 \times 29$	$43 \times 56 \times 35$
$\overline{Nu}$	19.493	19.570	19.577
Maximum component temperature	0.0158	0.0155	0.0159
Maximum wall temperature	0.00580	0.00564	0.00562
Maximum heat flux on the inner surface of the substrate	6.19×10^{-4}	6.15×10^{-4}	6.19×10^{-4}

Table 4 Definition of cases under study of vent locations

Case	Vent location	Number of vent(s)	Parameters fixed for all cases
Base case	Without vents	0	
Case-1	Right wall at $X = L_X$	1	$Ra = 10^6$
Case-2	Top wall at $Y = 3L_Y$	1	$S_V = 0.5$
Case-3	Bottom wall at $Y = 2L_Y$	1	$R_b = 38.45$
Case-4	Side wall at $Z = 0.5L_Z$ (placed symmetrically about $Z = 0$)	2	$R_s = 23.1$ $R_c = 7692.3$ geometry
Case-5	Top wall at $Y = 3L_Y$ and right wall at $X = L_X$	2	

Effect of vent locations

For cases 1–3, only one vent is employed, while a combination of two vents on different enclosure walls is considered for cases 4 and 5.

Figure 2 shows the velocity vectors for the various cases in the x–y plane. Strong boundary-layer-type flow along the surface of the substrate and the component is seen in all the cases. For the base case, the boundary-layer flow ascends along the substrate and its thickness becomes larger near the end region because of the confining top wall. The bulk flow in the core region exhibits a nearly uniform flow pattern of a very small velocity. For various vent locations, the flow patterns along the heated wall qualitatively do not change. The core region flow is, however, strongly influenced. In Figure 3, the 3-D effects are more evident.

For case 1, increased entrainment is seen near the bottom wall in Figures 2 and 3. The flow departs through the upper part of the vent. In the y–z plane, shown in Figure 3, a strong cell is generated in the lower half because of the interaction of the upflow and downflow along the side wall. Larger velocities are seen near the symmetry plane and along the bottom wall, as a result of the entrainment through the vent. Case 2 presents a dramatically distinct flow pattern effected by the vent on the top wall. A cooler air flow penetrates through the vent and makes a direct impact on the bottom wall. This flow behaves like a jet separating the enclosure flow into two regions. The strong entrainment from this jet-like flow strengthens the boundary-layer flow along the substrate, and a weak upflow is also generated along the right wall in the lower corner, as shown in Figures 2 and 3. It is also evident that a small part of the fluid entering through the vent does not contribute to the entrainment to the boundary-layer flow along the substrate and the component. A more complex flow field is observed in the y–z plane for case 2. The top vent induces a strong upflow in the upper end region near the symmetry plane, and a circulation still exists adjacent to the lower wall. When the vent is located on the bottom wall; i.e., for case 3, the flow pattern is nearly the same as that of the base case, except for the slight difference in the flow near the bottom wall, which is a result of the very weak inflow and outflow through the vent.

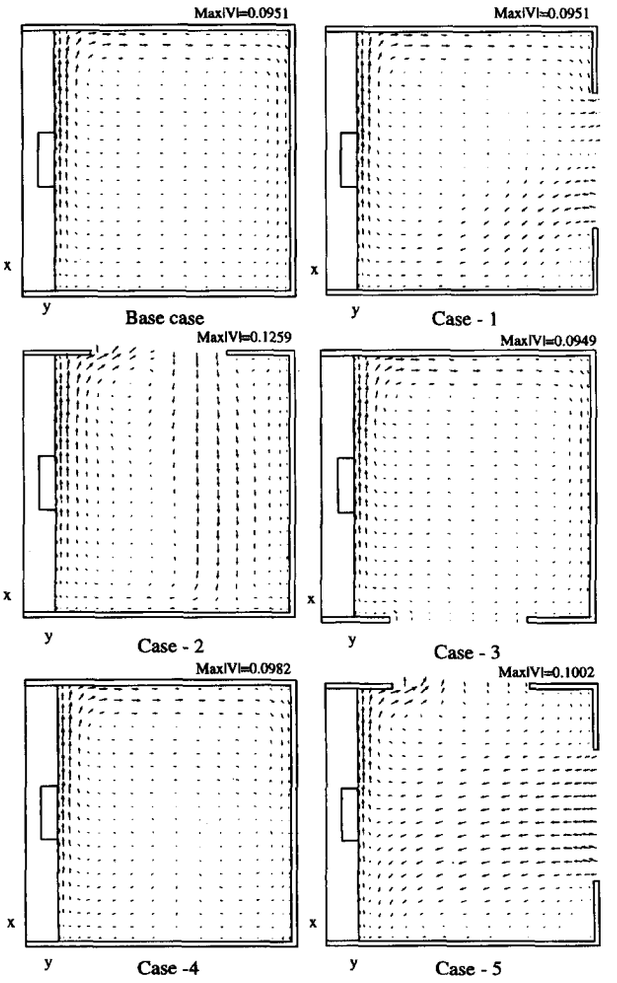

Figure 2 Velocity vectors in the x–y plane at $Z=0$ for different vent locations at Ra$=10^6$, $R_s=23.1$, and $S_v=0.5$

For case 4 and case 5, two vents are employed. First, for case 4, in the x–y plane, it is seen that the upper half of the flow field does not change much in comparison with the base case. In the lower region of the core, the flow spreads in all directions, indicating the existence of a flow source; i.e., the vent on the side wall. This effect is more prominant in the y–z plane. Case 5 exhibits a strong inflow pattern caused by the combination of vents on the top wall and the right wall. The inflow through the vent on the right wall impinges directly on the surface of the substrate and the component. The boundary-layer flow along the substrate is strengthened to be thinner and faster. Because of the large entrainment of cooler air from the vent on the right wall, there emerges a downflow adjacent to the boundary layer along the substrate, which does not exist in other cases. Also, the top vent provides the only escape path for the hot air, and the cooler air flows in through the vent on the right wall, which generates a flow pattern of larger nonunifom velocities in the interior region. A stronger upflow rises along the side wall and leaves the enclosure through the top vent, as shown in the y–z plane. This outflow forms a strong jet near the symmetry plane in the upper end region.

Figures 4 and 5 show the thermal responses for each of the above cases. Generally, in the fluid region, the thermal field consists of a thin boundary layer of large temperature gradients and interior regions of smaller temperature variations. It is also observed that the different vent locations do not affect the qualitative thermal patterns in the substrate significantly, which is dominated largely by the heat source. However, the changes in entrained flow for different vent positions effect the thermal patterns in the flow field.

For case 1, the stratified core region is disturbed by the entrainment and shifts up, leaving the lower region nearly isothermal. For case 2, the large temperature gradients are confined to the region adjacent to the substrate and the top wall. The interior region is formed of vertical isotherms spreading horizontally. In the y–z plane, a bay-like region is generated because of the entrainment from the vent on the top wall. Also, heat is transferred through the core region horizontally, and the temperature gradients near the side walls are reduced greatly because of the strengthened convection near the top wall. For case 3, the vent on the bottom wall has only a minor effect on the thermal distribution.

In case 4, as shown in Figure 4, the well-stratified core region also shifts to the upper end just as the situation in case 2, and results in a lower temperature zone directly above the bottom wall. For case 5, the whole thermal region is the combination of the boundary layer along the substrate and a uniform low temperature region in the core. In the y–z plane in Figure 5, it can still be observed that there exists a bay-like region in the upper end and a more uniform core region near the symmetry plane.

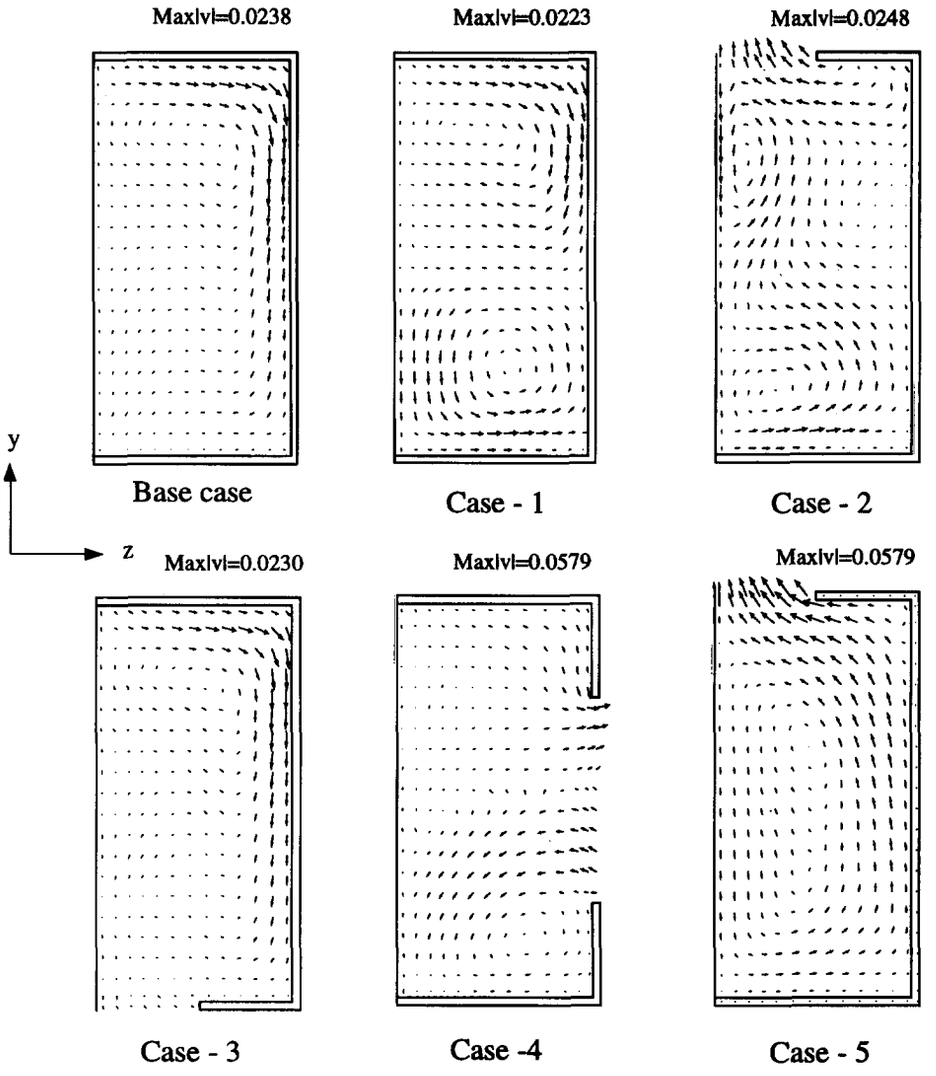

Figure 3 Velocity vectors in the y–z plane at $X = 2.5$ for different vent locations at $Ra = 10^6$, $R_s = 23.1$ and $S_v = 0.5$

Effect of vent size

Figure 6 documents the effect of vent sizes. For vent ratio $S_v = 0.2$, the entering flow turns around the lower edge of the vent and descends along the right wall. By referring to the base case in Figures 2 and 3, it is observed that the bulk flow of a small velocity in the interior region is not disturbed significantly by the weak entrainment. When the vent ratio is increased to $S_v = 0.7$, the large amount of cooler entering fluid directly reaches the substrate and the component through the core of the field, resulting in an upward shift of the well stratified region. By observing the flow pattern adjacent to the upper edge of the vent, it is evident that the departing flow turns around the corner and leaves the vent with a relatively small velocity for $S_v = 0.2$, while a larger escaping velocity is displayed for the large vent ratio $S_v = 0.7$. This is the result of increased entrainment through the wider opening.

Effect of Rayleigh number

Figure 7 presents the effect of Rayleigh numbers ranging from 10^4 to 10^6 for the fixed vent ratio $S_v = 0.5$ and $R_s = 23.1$. At $Ra = 10^4$, as shown in Figure 7a, a well-defined cell exists in the inner region. The boundary-layer flow characteristics are barely evident along the substrate. When Ra is increased to 10^5 and 10^6 in figures 7b and c, the circulation is no longer well defined, and the boundary-layer thickness adjacent to the heated wall decreases. When the temperature field is considered, the strong effects of Ra are also evident. A stratified core region is not observed at $Ra = 10^4$, but appears in the upper half of the enclosure for $Ra = 10^5$ and is clearer for $Ra = 10^6$. This leads to a uniform cooler zone near the bottom right corner. The boundary-layer flow above the heat source heats the substrate for $Ra = 10^6$, but at lower Ra, it is not the case. This is the result of lower temperatures of the substrate with specified relatively smaller R_s.

Effect of substrate thermal conductivity

The results of two levels of substrate thermal conductivity are presented for $Ra = 10^6$ and the vent on the right wall with the vent ratio $S_V = 0.5$ in Figures 8a and b. The velocity vectors in the x–y plane in Figure 8a display a thicker boundary layer along the substrate for $R_s = 5769.2$, which is attributable to the lower temperature in the substrate and the component resulting from the larger substrate thermal conductivity ratio. The overall flow patterns are similar for both cases. Also, in the x–y plane, the

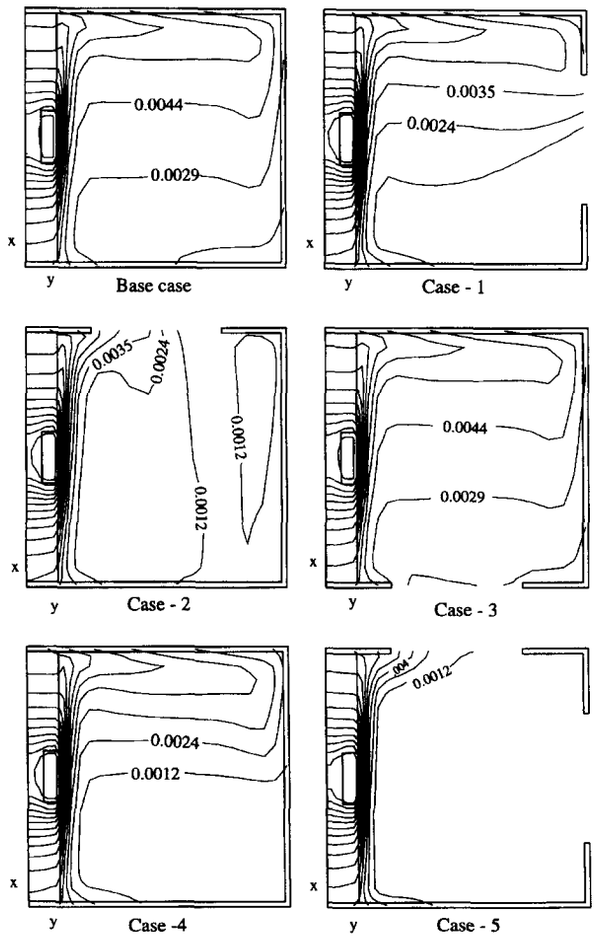

Figure 4 Isotherms in the x–y plane at $Z=0$ for different vent locations at Ra$=10^6$, $R_s=23.1$, and $S_v=0.5$

flow at the left bottom corner is more vigorous for lower R_s. This corresponds to the lower starting point of the thermal boundary layer, as indicated by the temperature distribution in Figure 8a, where the nearly uniform temperature in the substrate of a smaller thermal resistance heats up the air flow from the lower end of the enclosure, and it is also observed that the temperatures in the boundary layer exhibit an almost zero gradient in vertical direction for the same reason. A stratified core exists for the two cases, and the cold isothermal zone along the bottom wall is smaller for $R_S=5769.2$ because of the heating at the bottom end of the substrate. In the y–z plane in Figure 8b, the flow adjacent to the substrate surface provides a clear indication of the 3-D effect. For higher R_s, the increased spreading of heat induces an upflow of a nearly uniform velocity in z-direction. For $R_s=23.1$, the thermal footprint of the component is clearly visible and disappears because of spreading at higher R_s. Larger gradients are also observed near the enclosure walls for higher R_s.

Heat loss budget analysis

Figure 9 presents the heat loss budget from the surfaces of the component for different vent locations, Rayleigh numbers, and substrate thermal conductivity ratios. The definition of the names of surfaces of the component corresponds to the enclosure wall names by their orientations, except that the face of the component corresponds to the right wall, and the back of the component is the opposite surface. Generally, the heat loss into the substrate accounts for the largest fraction of the heat generated in the component, because of the high R_s considered in the present study. Less than 10% of the heat is directly carried away into the fluid through the face of the component. Also, the 3-D effect is very evident by observing the percentage heat loss from the two sides of the component.

Figure 9a shows the influence of vent locations on the heat loss fractions. The vent location, including the two combination cases, has a small effect, although case 5 generates a slightly higher percentage of heat loss from the component face to the air caused by the large mass flow rate. In Figure 9b, when Ra increases, the heat loss through the component face becomes more substantial, which is at the expense of the reductions of heat loss through other surfaces, especially the back of the component. This is because of the enhanced convection along the component face.

Figure 9c reveals that the thermal conductivity ratio of the substrate significantly affects the heat loss budget. At $R_s=5769.2$, a conduction-dominated regime emerges. This is indicated by the less than 2% of the heat being transferred through the face of the component into the flow, while this fraction is nearly 10% for $R_s=23.1$. For $R_s=23.1$, the sides of the component function as the path of the largest percentage heat loss, while the back releases the largest fraction of the heat for $R_s=5769$. When R_s increases, the temperature variation rises near the top, producing an increased percentage heat loss from the top, and it decreases near the bottom, generating a declined heat loss fraction from the bottom, as shown in Figure 9c. For both thermal conductivity ratios, the sides of the component play a substantial role in transferring the heat, indicating that the 3-D effects cannot be neglected in the present situation.

Local and overall heat transfer, maximum temperatures, and mass outflow rates

The local and overall heat transfer for the cases studied are presented in terms of local and average Nusselt numbers. In addition, the temperatures along the component/fluid and substrate/fluid interfaces, and the mass outflow rates are also computed. They are determined in the following manner:

$$\mathrm{Nu}=\frac{L_X}{\theta_{\mathrm{sur}}}\left(-\frac{\partial\theta}{\partial X}\right)_{\mathrm{sur}}$$

$$\overline{\mathrm{Nu}}=\frac{2}{L_Y\theta_{\mathrm{sur}}}\int\int\left(-\frac{\partial\theta}{\partial X}\right)_{\mathrm{sur}}\mathrm{d}Y\,\mathrm{d}Z$$

$$\theta_{\mathrm{sur}}=\frac{(\delta X_s/R_s)\theta_f+(\delta X_f/R_f)\theta_s}{(\delta X_s/R_s)+(\delta X_f/R_f)}$$

$$M_{\mathrm{out}}=\int URa^{1/2}\mathrm{d}Y\,\mathrm{d}Z$$

where

$$U=U_{X=L_X}\quad\text{for}\quad U_{X=L_X}>0$$

$$U=0\quad\text{for}\quad U_{X=L_X}\le 0$$

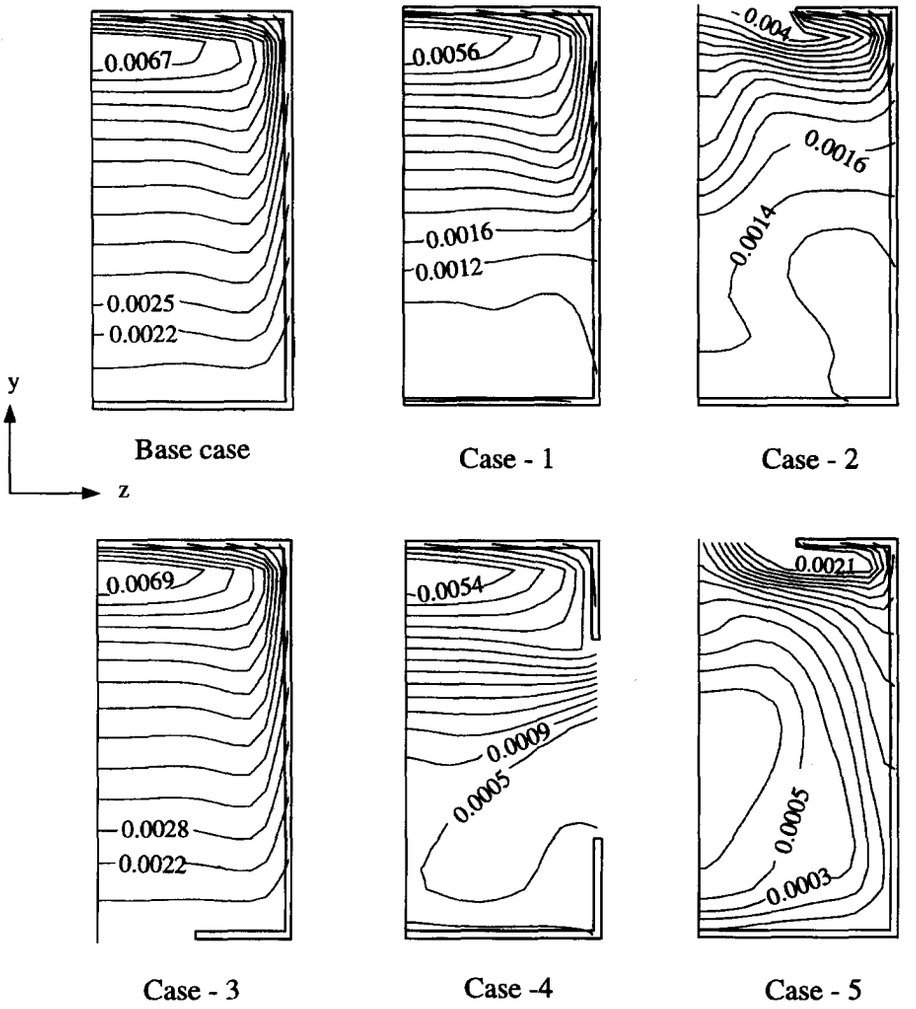

Figure 5 Isotherms in the y–z plane at $X=2.5$ for different vent locations at Ra$=10^6$, $R_s=23.1$, and $S_v=0.5$

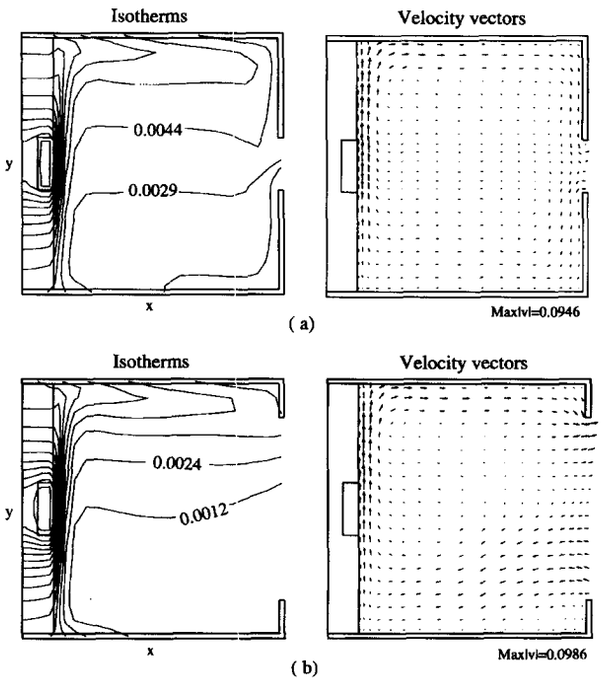

Figure 6 Isotherms and velocity vectors in the x–y plane at $Z=0$ for different vent sizes Ra$=10^6$, $R_s=23.1$; (a) $S_v=0.2$, (b) $S_v=0.7$

In the definition of θ_{sur}, T_f and T_s are the fluid and solid temperatures at the nodes closest to the interface, and δX_s and δX_f are their distances normal to this interface. When the component is involved, the subscript s is replaced by c, and the corresponding values of the component are used. In the definition of M_{out}, when the vent is located on other walls, a similar formula is used by replacing U with the velocity component normal to the wall with that vent.

Table 5 shows how the vent locations affect the heat transfer in the enclosure. For case 3, all the parameters except M_{out} are nearly same as those of the base case. This is because of the stratified region of lower temperatures and small velocities near the bottom wall, so the vent does not generate much influence on the internal heat transfer. Case 1 and case 2 introduce larger average Nusselt numbers than the base case. It is observed that case 2 does not produce higher heat transfer from the component than case 1, and only a lower wall temperature emerges, as a result of the flow pattern in Figure 2. For cases 4 and 5, effects of vents become stronger than for one-vent cases. It is interestingly seen that the two vents on side walls for case 4 generate slight increases of local and average Nusselt numbers over case 1 and case 2, which indicates that vents on side walls fail to enhance the heat transfer from the heat source, as the large mass flow rate suggests. This result is because some of the mass flow does not contribute to the entrainment to the boundary-layer flow along the substrate. A part of the inflow turns to the right wall, rises along it, and finally leaves the enclosure through the upper region of the vents. Case 5 gives rise to the largest local

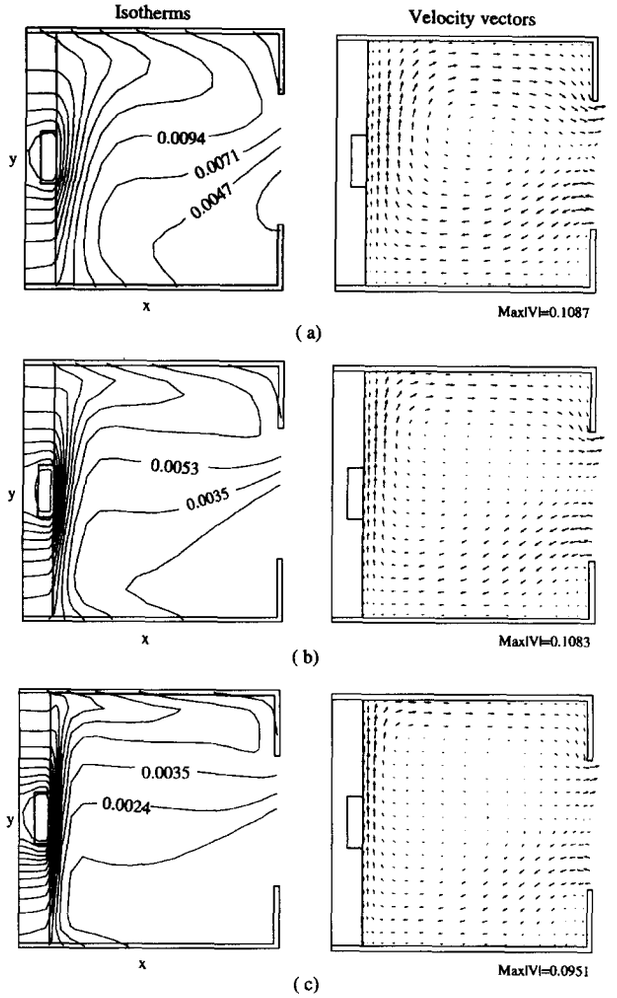

Figure 7 Isotherms and velocity vectors in the x–y plane at $Z=0$ for different Rayleigh numbers at $S_v=0.2$, $R_s=23.1$, (a) $Ra=10^4$ (b) $Ra=10^5$ (c) $Ra=10^6$

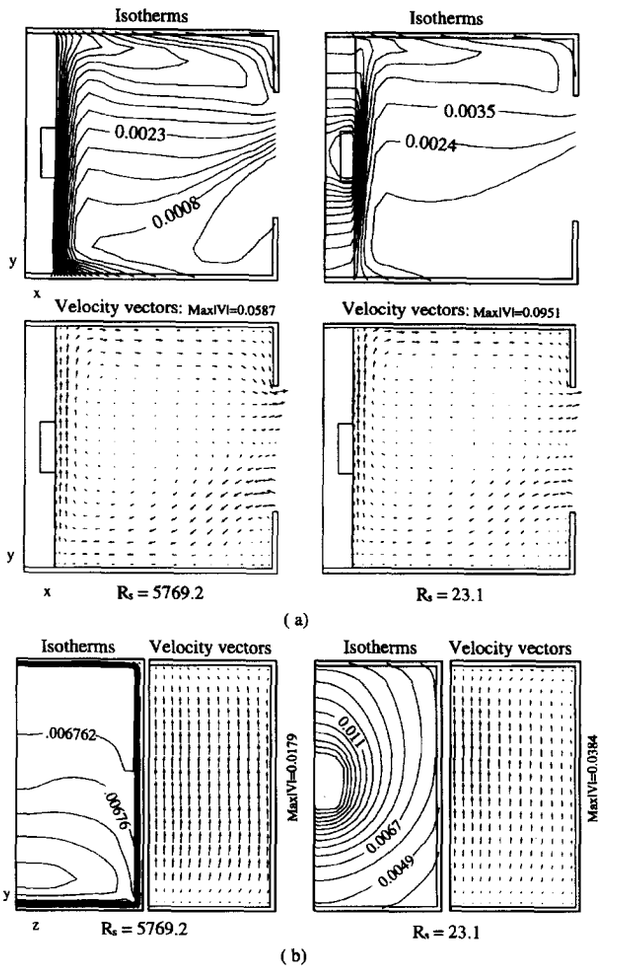

Figure 8 Isotherms and velocity vectors for different substrate thermal conductivity ratios at $S_v=0.2$, $Ra=10^6$; (a) x–y plane at $Z=0$ (b) y–z plane at $X=0.625$

and overall heat transfer as indicated by the values in Table 5, which is in agreement with the flow and thermal patterns shown in Figures 2–5.

The effect of vent sizes on the heat transfer is presented in Figure 10 for $Ra=10^5$ and $Ra=10^6$. It is revealed that the average Nusselt number increases more than 30% for the vented enclosure of $S_v=1.0$ over the sealed one, resulting in a decrease in the maximum component temperature, especially rapidly for the vent ratio between $S_v=0.2$ and $S_v=0.5$. It is also seen that the effect of vent sizes becomes somewhat less pronounced when Ra is reduced. At $Ra=10^6$, the percentage of reduction of θ_{max} is 9.6%, while a 9.1% decrease is for $Ra=10^5$, when S_v changes from 0 to 1.0. This seems to be because for higher Ra, the boundary-layer flow dominates the removal of heat from the surfaces of the substrate and the component, which is substantially affected by the inflow mass rate. For lower Ra, the internal bulk flow contributes much to the convection, which is less influenced by the through-flow mass induced by the weaker buoyancy.

Figure 11 presents the heat transfer results in terms of Nusselt number and the temperatures on the surfaces of the substrate and the component. Figure 11a, b, and c, complemented by Table 6, show the local heat transfer results at different Ra for the right wall vents for $S_v=0.5$ and $R_s=23.1$. It is observed that the patterns of temperature along the surfaces of the substrate, and the components are nearly same for different Ra, which is the result of high R_s. However, the nondimensional temperatures decrease significantly because of the stronger convection effects corresponding to higher Ra.

It is seen that the lowest Nusselt number at $Ra=10^4$ exists along the surface of the substrate, above the flush component. With increasing Ra, this region becomes smaller, as 3-D effects get stronger. At $Ra=10^6$, in Figure 11c, a negative Nu region emerges in the upper left corner, meaning that the plume heats the substrate there. This is in conformity with the thermal pattern in Figure 4. It is also evident that Nu is larger near the side edge of the component, especially for $Ra=10^4$ because of the large temperature gradient in the substrate adjacent to the sides of the component, resulting in a cooler boundary layer flow than at the center of the component. As for the maximum Nusselt number, it occurs generally on the bottom edge of the component, resulting from the thinnest boundary layer there.

In Figure 11d, the contours are obtained based on the same conditions as those of the results shown in Figure 11c, except for $R_s=5769.2$. The maximum component temperature decreases 64% when R_s increases from 23.1 to 5769.2, as seen in Table 7. The wall temperatures are also decreased. The smaller average

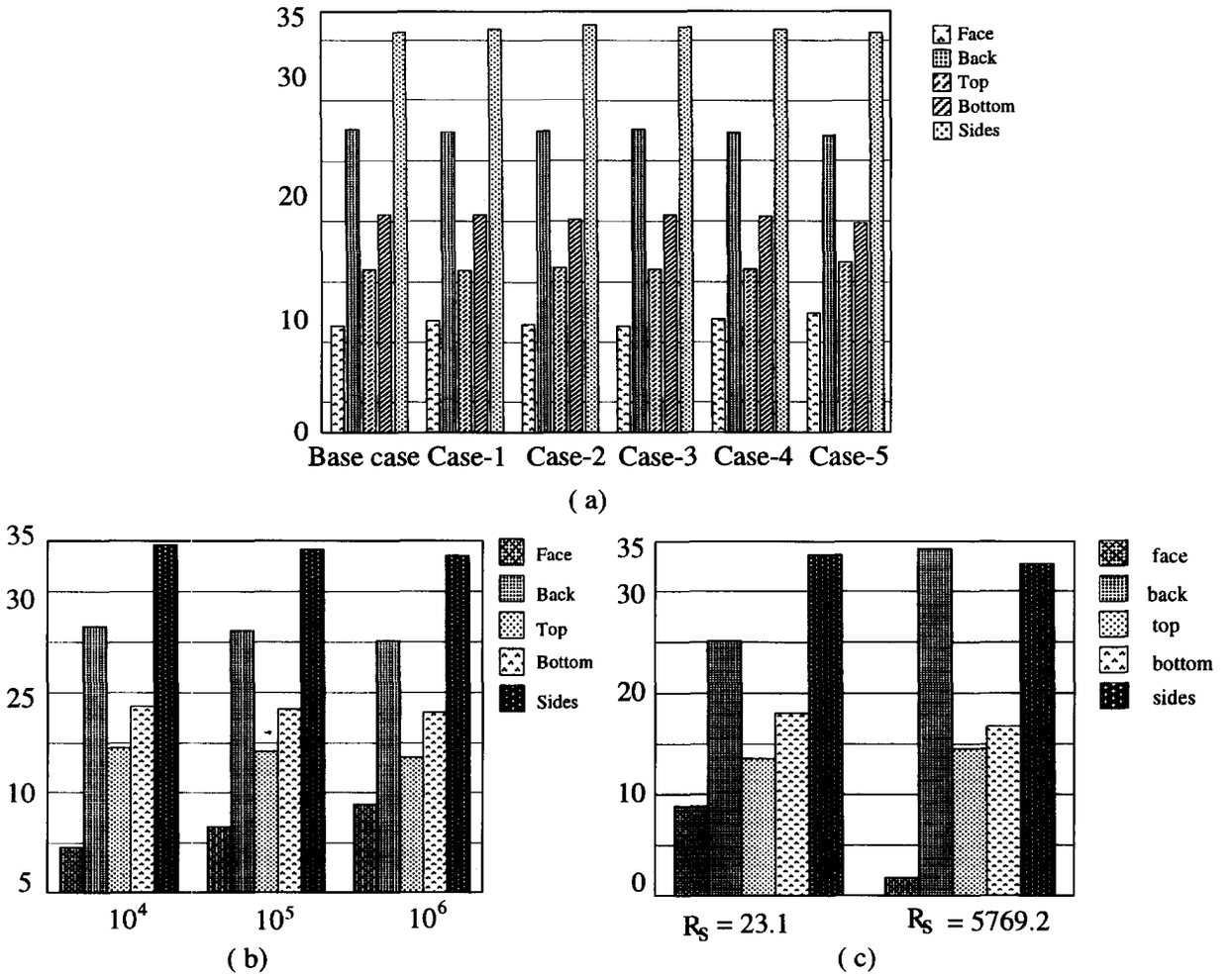

Figure 9 Heat loss budget of the component for different conditions; (a) effect of vent location at Ra=10^6, R_s=23.1 and S_v=0.5; (b) effect of Raleigh number at R_s=23.1 and S_v=0.5 and the right vent; (c) effect of substrate thermal conductivity ratio at Ra=10^6 and the right vent of S_v=0.5

Nusselt number for the higher R_s indicates a less pronounced convection mode in the fluid. Two interesting characteristics are seen in the Nu contours. The maximum Nu shifts down near the left bottom corner, as shown in Figure 11d for $R_s = 5769.2$, in comparison with the lower R_s case, where it exists near the bottom edge of the component. Secondly, the region of negative Nu seen for $R_s = 23.1$ disappears for higher $R_s = 5769.2$ and is replaced with a distribution of horizontally uniform Nu above the component. Both of these characteristics are a result of the increased spreading of the heat in the substrate.

The average convective coefficients on the component surface were also obtained for the simplified models using the correlations for a vertical flat plate and with approximate boundary conditions specified on the opening. The geometry is similar to that in Figure 1, with adiabatic side, top, and bottom walls and a complete opening opposite the substrate. The approximate boundary conditions on the opening are the same as those for the extended domain at $X = 3Lx$ except for $V = W = 0$. Two aspect ratios of the enclosure were considered.

Table 5 Local and overall heat transfer for different vent locations at Ra=10^6, S_v=0.5, R_s=23.1

	$\overline{Nu}$	θ_{max}	θ_b	M_{out}	Nu_{max}
Base case	9.28	0.0209	0.00977	0.0	27.30
Case 1	11.49	0.0196	0.00875	50.2	30.38
Case 2	11.43	0.0196	0.00854	65.1	29.65
Case 3	9.27	0.0209	0.00980	7.8	27.21
Case 4	11.75	0.0195	0.00850	153.0	30.71
Case 5	12.12	0.0187	0.00758	134.3	31.67

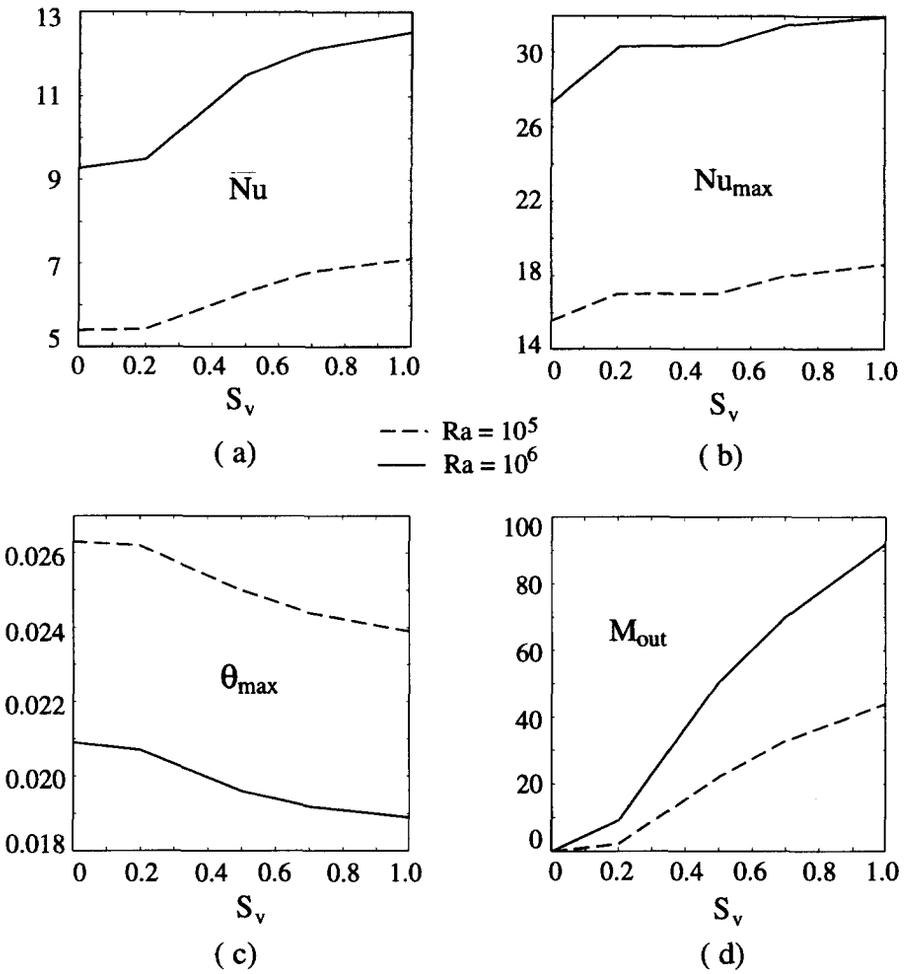

Figure 10 Effect of vent size on the local and overall heat transfer for R_s = 23.1 and the right vent

The results shown in Table 8 and computed flow and temperature patterns reveal that the approximate boundary conditions cannot accurately predict the average heat transfer coefficient on the component or the 3-D temperature and flow patterns at the opening, especially for higher aspect ratios, although they can model the maximum component temperature to a good degree of accuracy. Therefore, for estimations of component temperatures, these approximate boundary conditions may be used to save on computing resources; however, for understanding the 3-D natural convection and radiation, they are not sufficient. It is also found the significant errors, up to 57%, are introduced, using the correlation for the vertical flat plate by Churchill and Chu (1975). The surface temperatures used in the correlation are those from extended domain computations.

Conclusions

A 3-D numerical study of natural-convection cooling of a heat-generating component in vented enclosures is carried out. The following conclusions are obtained.

(1) The vent locations significantly affect the 3-D flow and thermal fields within the enclosure. For one-vent case, the vents on the top wall and on the right wall of the enclosure give a similar cooling effect of the heat source, but generate very different flow and temperature patterns in the fluid. The vent of the bottom wall results in nearly no enhancement of cooling over the sealed enclosure case. The vent on the side wall can contribute to the convection effect but not as much as the vents on the top and right walls do. The combination of vents on the top and right walls provides the largest cooling effect for the present study.

(2) The vent size influences the natural convection. At Ra = 10^6, the maximum temperature of the component is reduced nearly 10% over the sealed enclosure when a vent of $S_v = 1.0$ is employed on the right wall. The cooling effect of vent sizes becomes more prominent with increasing Ra.

(3) The average Nusselt number for Ra = 10^6 is nearly 2.5 times greater than that for Ra = 10^4.

(4) The substrate thermal conductivity plays an important role in the cooling.

(5) Heat loss budget analysis of the component reveals that the substrate transfers most of the heat generated in the heat source. The 3-D effect is very pronounced, evidenced by the large percentage of heat loss through the sides of the component.

(6) The simplified model using the correlation for the vertical flat plate results in significant errors up to 57%. The approximate boundary conditions result in good predictions of the component temperatures, but not of the flow and temperature fields.

Acknowledgments

The authors acknowledge support for this work through the Maryland Industrial Partnerships Program (MIPS).

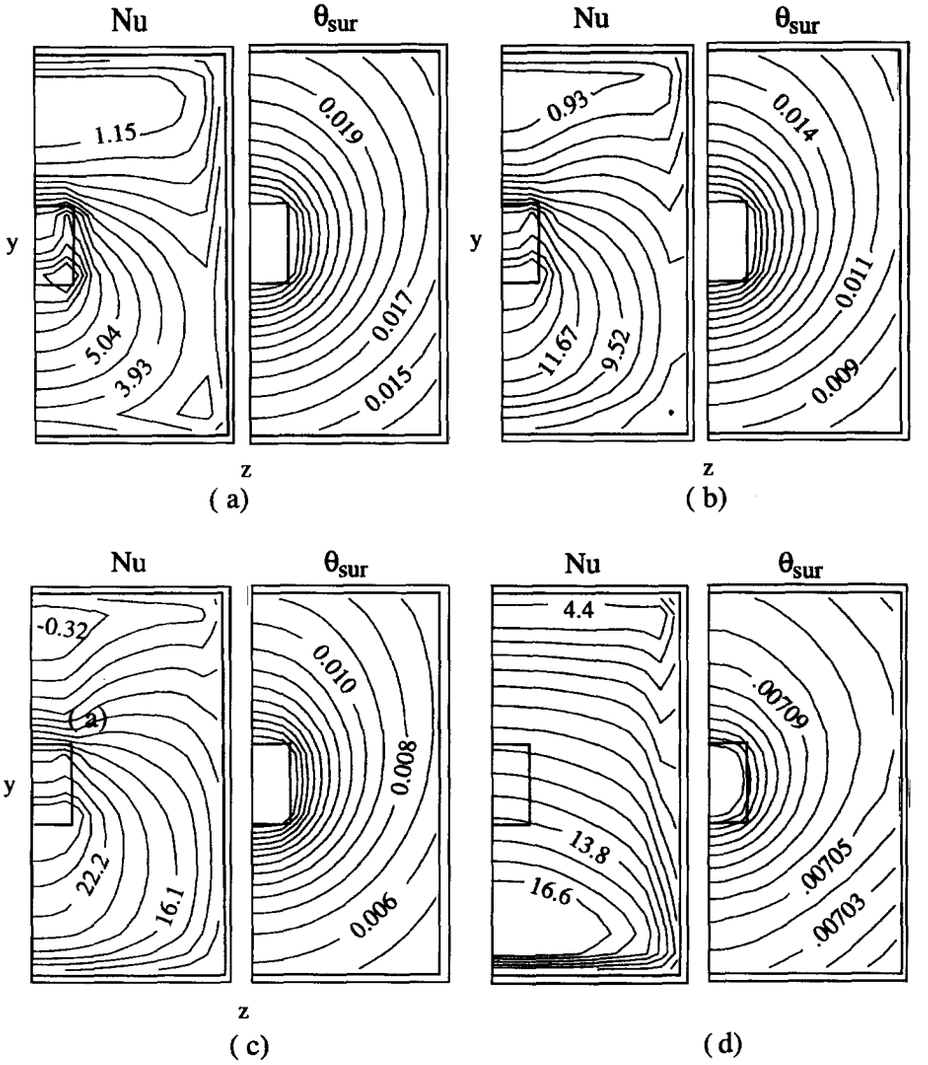

Figure 11 Contours of Nusselt number and temperatures on the surfaces of the substrate and the component for different Ra and R_s for the right vent at $S_v=0.5$; (a) Ra=10^4, Rs=23.1; (b) Ra=10^5, Rs=23.1; (c) Ra=10^6, Rs=23.1; (d) Ra=10^6, Rs=5769.2

Table 6 Local and overall heat transfer for different Rayleigh numbers at $S_v=0.5$, $R_s=23.1$

Ra	$\overline{Nu}$	θ_{max}	θ_b	M_{out}	Nu_{max}
10^4	3.30	0.0314	0.00190	7.3	9.52
10^5	6.31	0.0250	0.00131	22.1	17.04
10^6	11.49	0.0196	0.00875	50.2	30.38

Table 7 Local and overall heat transfer for different substrate thermal conductivity ratios at Ra=10^6, $S_v=0.5$

Rs	Nu	θ_{max}	θ_b	M_{out}	Nu_{max}
5769.2	9.95	0.0071	0.00704	50.5	18.44
23.1	11.49	0.0196	0.00875	50.2	30.38

Table 8 Average $\bar{h}$(W/m^{2}K) on the component surface for two levels of Ra

Ra	$Q(W)$	Correlation	Actual domain	Extended domain	Aspect ratio
10^6	0.72	8.97	6.34	6.00	4
2×10^6	1.5	11.0	7.7	7.00	4
10^6	0.72	8.98	5.98	5.91	1
2×10^6	1.5	10.4	7.12	6.75	1

References

Abib, A. H. and Jaluria, Y. 1988. Numerical simulation of the buoyancy-induced flow in a partially open enclosure. *Numer. Heat Transfer* **14**, 235–254

Abib, A. H. and Jaluria, Y. 1992. Penetrative convection in a partially open enclosure in Natural Convection in Enclosures, Proc. 28th National Heat Transfer Conference and Exhibition, San Diego, CA, P. G. Simpkins, R. S. Figliola, and J. G. Georgiadis, Eds. HTD, Vol. 198, ASME, New York, 73–81

Abib, A. H. and Jaluria, Y. 1993. Generation of stable thermal stratification by turbulent flows in a partially open enclosure in Fundamentals of Natural Convection, Proc. 1993 ASME Winter Annual Conference, New Orleans, LA, R. D. Boyd and P. G. Kroeger, Eds. HTD, Vol. 264, ASME, New York, 127–140

Angirasa, D., Pourquie, M. J. B. M. and Nieuwstadt, F. T. M. 1992. Numerical study of transient and steady laminar buoyancy-driven flows and heat transfer in a square open cavity. *Numer. Heat Transfer*, **22**, 223–239

Chan, Y. L. and Tien, C. L. 1985. A numerical study of two-dimensional laminar natural convection in shallow open cavities. *Int. J. Heat Mass Transfer*, **28**, 603–612

Chan, Y. L. and Tien, C. L. 1986. Laminar natural convection in shallow open cavities. *J. Heat Transfer*, **108**, 305–309

Churchill, S. W. and Chu, H. H. S., 1975. Correlating equations for laminar and turbulent free convection from a vertical plate. *Int. J. Heat Mass Transfer*, **18**, 1323–1329

Dehghan, A. A. 1994. Natural convection in a discretely heated open cavities. Ph.D. thesis, The University of New South Wales,

Dehghan, A. A. and Behinia, M. 1996. Combined natural convection–conduction and radiation heat transfer in a discretely heated open cavity. *J. Heat Transfer*, **118**, 56–64

Gebhart, B., Jaluria, Y., Mahajan, R. L. and Sammakia, B. 1988. *Buoyancy-Induced Flows and Transport*. Hemisphere Publishing, Bristol, PA, 797–798

Karki, K. C., Sathyamurthy, P. S. and Patankar, S. V. 1992. Natural convection in a partitioned cubic enclosure. *J. Heat Transfer*, **114**, 410–417

Kelkar, K. M. and Patankar, S. V. 1990. Numerical prediction of natural convection in square partitioned enclosures. *Numer. Heat Transfer*, **17**, 269–285

Mallinson, G. D. and de Vahl Davis, G. 1977. Three-dimensional natural convection in a box, A numerical study. *J. Fluid Mech.*, **83**, 1–31

Miyamoto, M., Kuehn, T. H., Goldstein, R. J. and Katoh, Y. 1989. Two-dimensional laminar natural convection heat transfer from a fully or partially open square cavity. *Numer. Heat Transfer*, **15**, 411–430

Myrum, T. A. 1990. Natural convection from a heat source in a top-vented enclosure. *J. Heat Transfer*, **112**, 632–639

Olson, D. A., Glicksman, L. R. and Ferm, H. M. 1990. Steady-state natural convection in empty and partitioned enclosures at high Rayleigh numbers. *J. Heat Transfer*, **112**, 640–647

Patankar, S. V. 1980. *Numerical Heat Transfer and Fluid Flow*, Hemisphere, Bristol, PA, 1090–1093

Sefcik, D. M., Webb, B. W. and Heaton, H. S. 1991. Natural convection in vertically vented enclosures. *J. Heat Transfer*, **113**, 912–918

Xia, J. L. and Zhou, Z. W. 1992. Natural convection in a partially open cavity with a divide. *Int. Comm. Heat Mass Transfer*, **19**, 447–460